Supporting Information

Hydrolysis of Ammonia Borane Catalyzed by NiCoP/OPC-300 Nanocatalysts: High Selectivity, Efficiency and Mechanism

Xiaopeng Qu, [a] Rui Jiang, [a] Qian Li,[a] Fanan Zeng,[a] Xue Zheng,[a] Zhimou Xu,[a, *] Cunhua Chen[b] and Jing Peng[c]

[a] Wuhan National Laboratory for Optoelectronics, School of Optical and Electronic Information, Huazhong University of Science and Technology, Wuhan 430074, China.

[b] Department of Chemistry, Central China Normal University, Wuhan 430079, PR China.

[c] College of Science, Wuhan University of Science and Technology, Wuhan 430081, China.

†Electronic supplementary information (ESI) available.

*Corresponding author. E-mail: Xuzhimou@mail.hust.edu.cn

1. Chemicals and materials

All chemicals were commercial and used without further purification. Cobalt nitratehexahydrate ($Co(NO_3)_2 \cdot 6H_2O$,99%), 2-methylimidazole (2-MeIM, 98%), cobalt chloride hexahydrate ($CoCl_2 \cdot 6H_2O$, 99%), Nickel chloride hexahydrate ($NiCl_2 \cdot 6H_2O$, 99%), sodium hypophosphite (NaH_2PO_2, 99%),sodium borohydride ($NaBH_4$, 98%), methanol (CH_3OH, >99.8%) and ethanol (C_2H_5OH, >99.8%) were supplied by Wuhan Greatwall Chemical company. Ultrapure water with the specific resistance of 18.3 MΩ·cm was used as the reaction solvent.

2. Physical characterizations

Powder X-ray diffraction (XRD) patterns were measured by a Bruker D8-Advance X-ray diffractometer using Cu Kα radiation source (λ = 0.154178 nm) with a velocity of 10^o min^{-1}. The morphologies and sizes of the samples were observed by using a Tecnai G20 U-Twin transmission electron microscope (TEM) at an acceleration voltage of 200 kV and a Titan G2 60-300 Titan Probe corrected TEM equipped with an energy dispersive X-ray detector (EDX) at an acceleration voltage of 300 kV. X-ray photoelectron spectroscopy (XPS) measurement was performed with a Thermo Fischer ESCALAB 250Xi spectrophotometer. Inductively coupled plasma-atomic emission spectroscopy (ICP-AES) was performed on IRIS Intrepid II XSP. The characterization of Brunauer-Emmett-Teller (BET) surface data, which was based on N_2 adsorption/desorption

isotherms at 77 K and controlled by liquid nitrogen, was measured using a Quantachrome NOVA 4200e.

3. The pathways of AB hydrolytic dehydrogenation

The pathways of AB hydrolytic dehydrogenation are as follows:

$$H_3BNH_3 + * \longrightarrow H_3BNH_3* \quad \text{S3-1}$$

$$H_2O + * \longrightarrow H_2O* \quad \text{S3-2}$$

$$OH*+H_3BNH_3* \longrightarrow H_3BOH* + NH_3* \quad \text{S3-3}$$

$$BH_3OH* \longrightarrow BH_2OH* + H* \quad \text{S3-4}$$

$$BH_3OH* + OH* \longrightarrow BH_2(OH)_2* + H* \quad \text{S3-5}$$

$$BH_2OH* \longrightarrow BHOH*+ H* \quad \text{S3-6}$$

$$BH_2OH* + H_2O* \longrightarrow BHOH*+H_2*+ OH* \quad \text{S3-7}$$

$$BH_2OH*+ OH* \longrightarrow BH_2(OH)_2* \quad \text{S3-8}$$

$$BH_2OH* + NH_3* \longrightarrow HOBH_2\text{-}NH_3* \quad \text{S3-9}$$

$$OH*+ HOBH_2\text{-}NH_3* \longrightarrow BH_2(OH)_2*+ NH_3* \quad \text{S3-10}$$

$$H_2O*+ H* \longrightarrow OH*+ H_2* \quad \text{S3-11}$$

$$H_2* \longrightarrow H_2(g) \quad \text{S3-12}$$

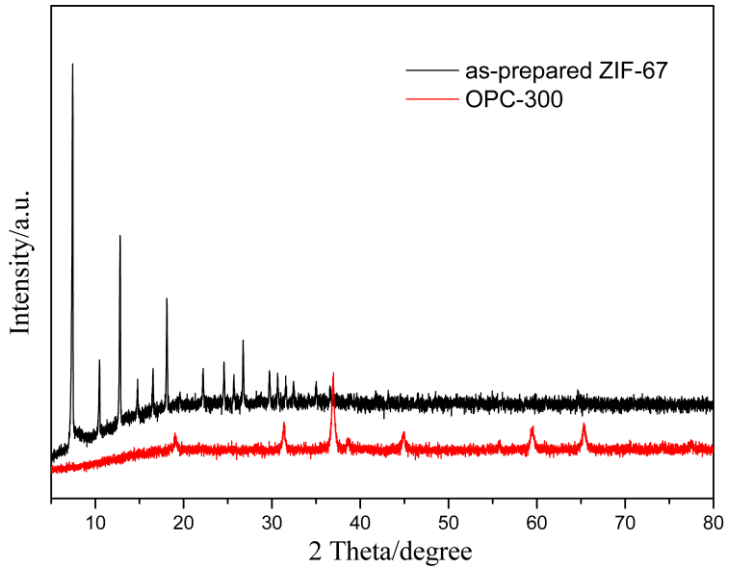

Fig.S1 Powder XRD patterns of the obtained (a) as-prepared ZIF-67;(b)the OPC-300.

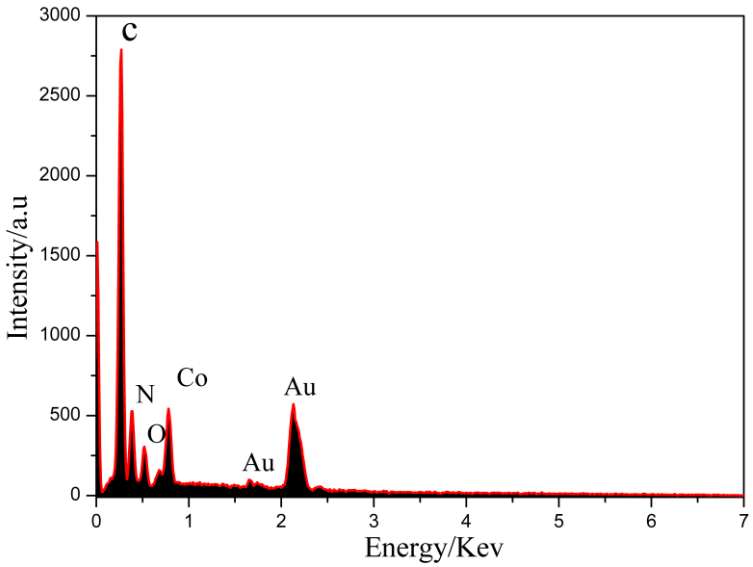

Fig.S2 the corresponding EDX spectrum of as-prepared ZIF-67.(The Au signal originates from the sputtering Au particles.)

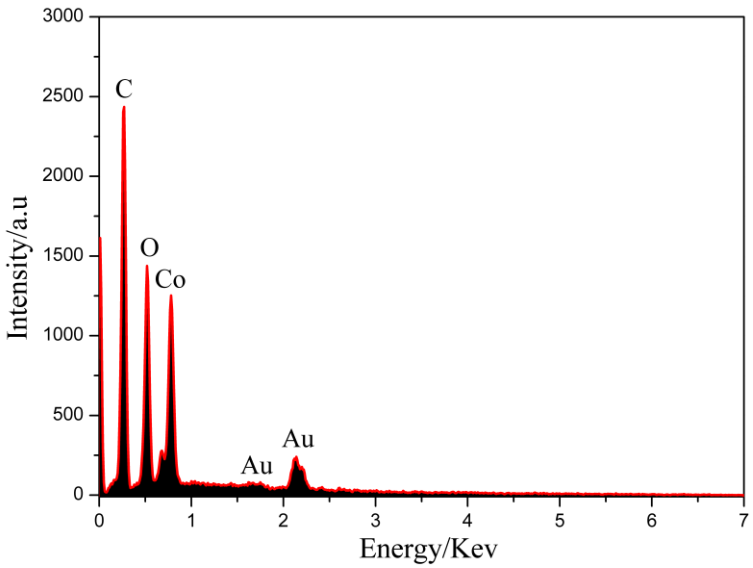

Fig.S3 the corresponding EDX spectrum of the OPC-300.(The Au signal originates from the sputtering Au particles.)

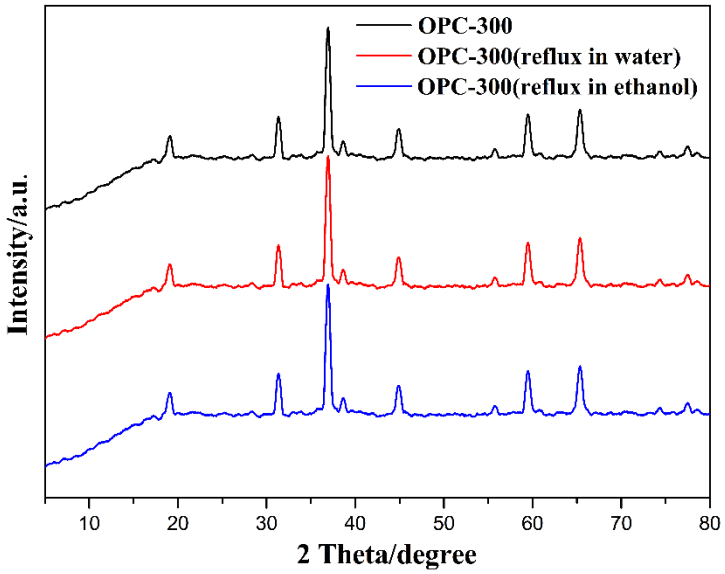

Fig.S4 PXRD patterns of as-synthesized OPC-300 and OPC-300 refluxing in water or ethanol two days.

Table S1. Physical Properties of the Nanocatalysts on OPC-300.

Sample	BET surface area(m^2/g)	pore volume(cm^3/g)
ZIF-67	1371.33	0.5968
OPC-300	56.21	0.3882
$Ni_{0.66}Co_{0.19}P_{0.15}$/OPC-300	37.3	0.3572

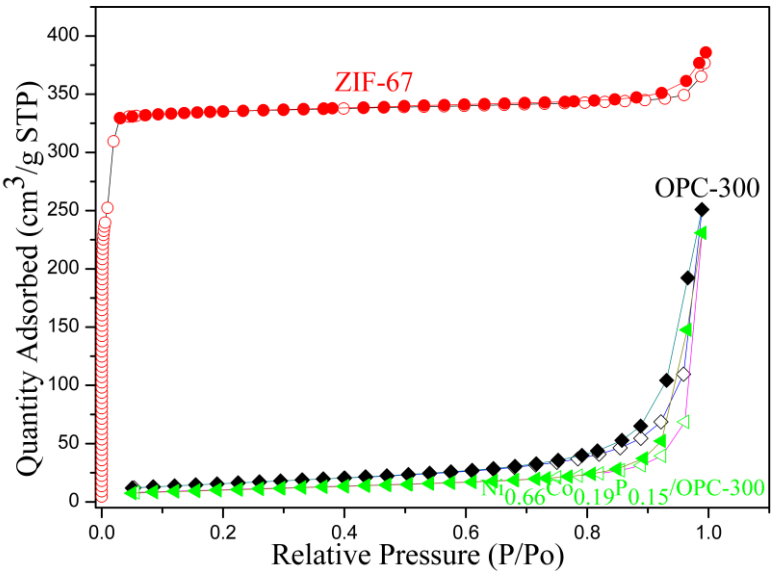

Fig.S5 N_2 adsorption-desorption isotherms of the ZIF-67, OPC-300 and $Ni_{0.66}Co_{0.19}P_{0.15}$/OPC-300.

Table S2. Reactant molar ratios and ICP results for the synthesis of various samples

Catalysts	Initial molar ratios			ICP results			
	$NiCl_2$	$CoCl_2$	NaH_2PO_2	Ni (wt.%)	Co (wt.%)	P (wt.%)	Ni:Co:P (at.%)
$Ni_{0.75}Co_{0.25}$/OPC-300	0.04	0.01	0	23.476	5.893	0	0.75:0.25
$Ni_{0.68}Co_{0.21}P_{0.11}$/OPC-300	0.04	0.01	0.1	17.9	4.42	3.72	0.68:0.21:0.1 1
$Ni_{0.66}Co_{0.19}P_{0.15}$/OPC-300	0.04	0.01	0.2	19.37	5.6	2.32	0.66:0.19:0.1 5
$Ni_{0.65}Co_{0.17}P_{0.18}$/OPC-300	0.04	0.01	0.3	16.43	3.83	4.805	0.65:0.17:0.1 8
$Ni_{0.64}Co_{0.15}P_{0.21}$/OPC-300	0.04	0.01	0.4	15.85	3.53	5.09	0.64:0.15:0.2 1

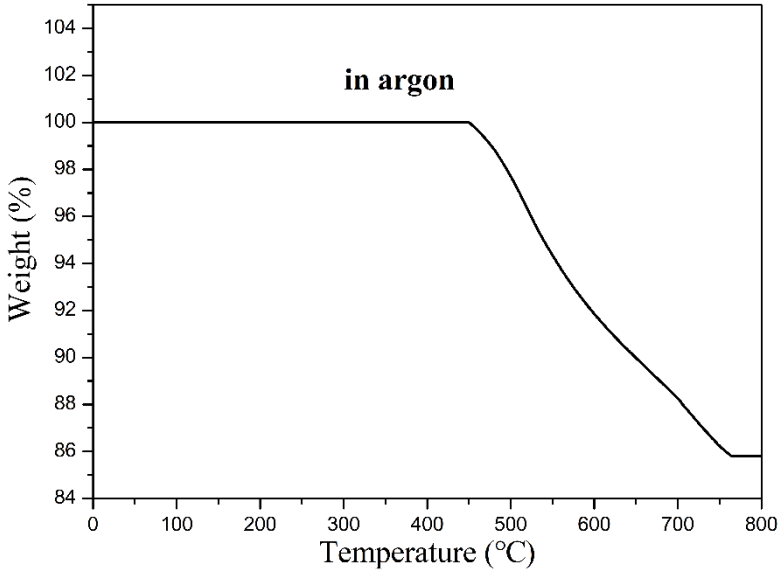

Fig.S6 Thermogravimetric analysis (TGA) curves of the prepared $Ni_{0.66}Co_{0.19}P_{0.15}$/OPC-300 nanocatalysts with a ramp of 5 ℃/min.

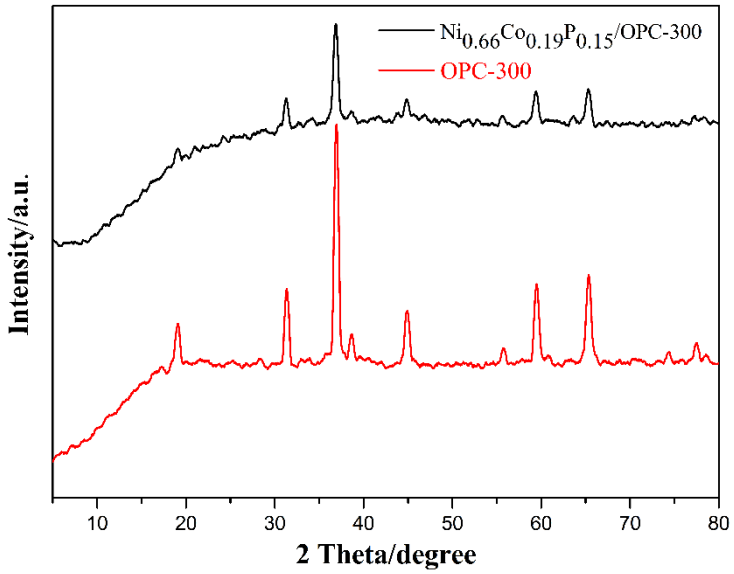

Fig.S7 Powder XRD patterns of the obtained (a) the OPC-300; (b) the $Ni_{0.66}Co_{0.19}P_{0.15}$/OPC-300.

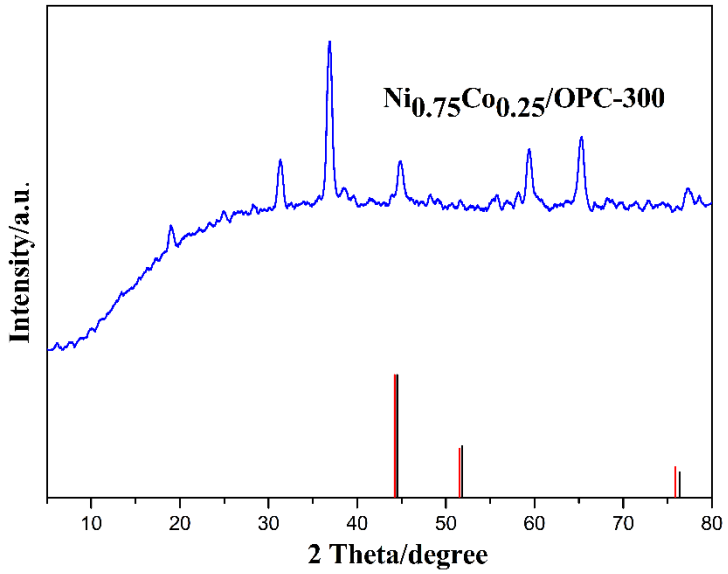

Fig.S8 Powder XRD patterns of the obtained $Ni_{0.75}Co_{0.25}$/OPC-300. (the red line:Co-PDF#15-0806; the black line: Ni-PDF#04-0850);

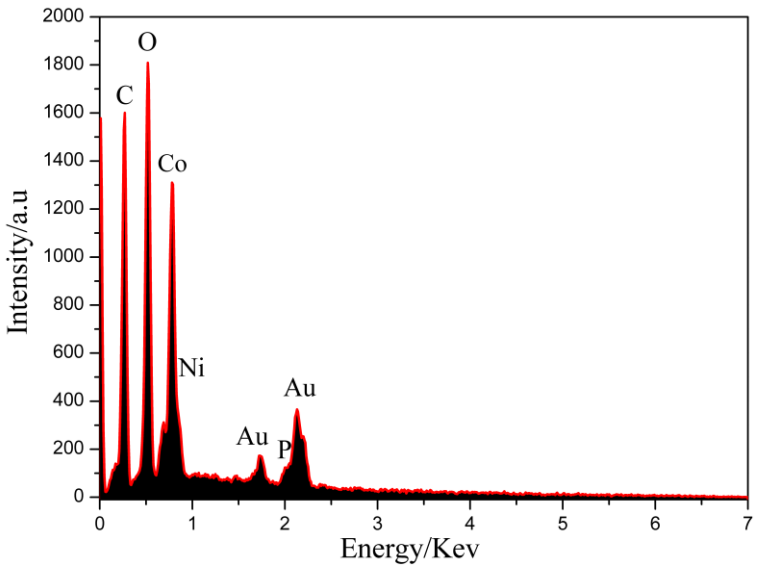

Fig.S9 the corresponding EDX spectrum of the $Ni_{0.66}Co_{0.19}P_{0.15}$/OPC-300.(The Au signal originates from the sputtering Au particles.)

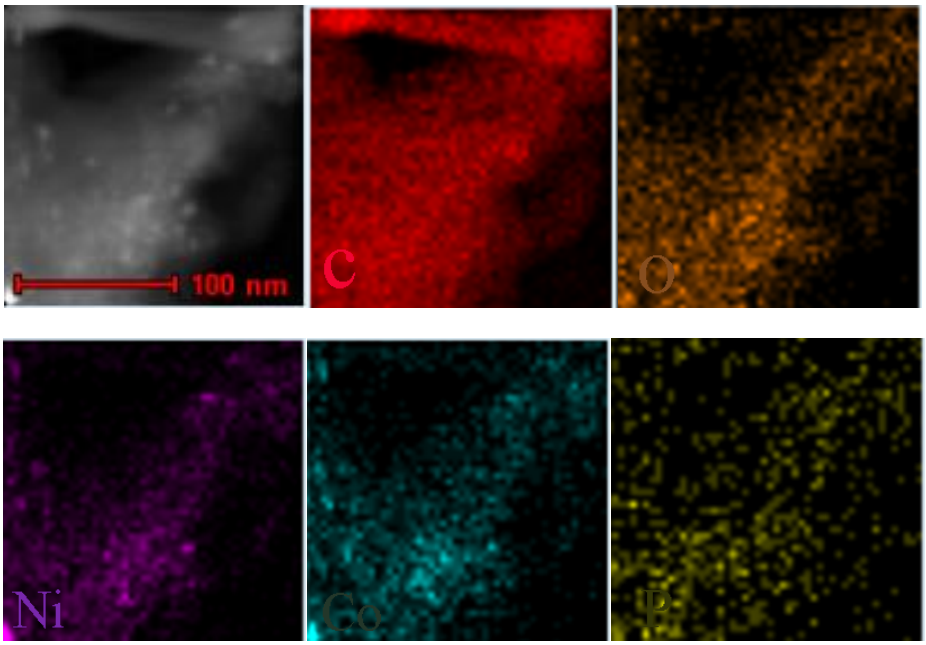

Fig.S10 HADDF-STEM and EDX mapping images of the $Ni_{0.66}Co_{0.19}P_{0.15}$/OPC-300.

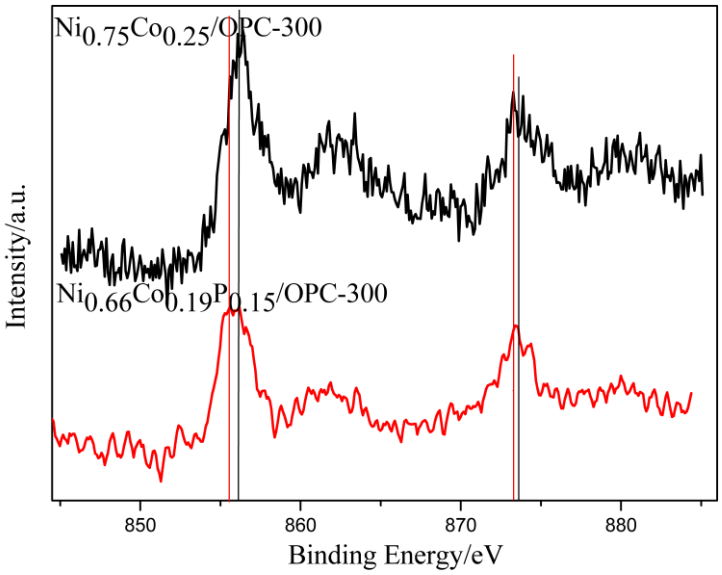

Fig.S11 Ni 2p XPS spectra of $Ni_{0.66}Co_{0.19}P_{0.15}$/OPC-300 and $Ni_{0.75}Co_{0.25}$/OPC-300.

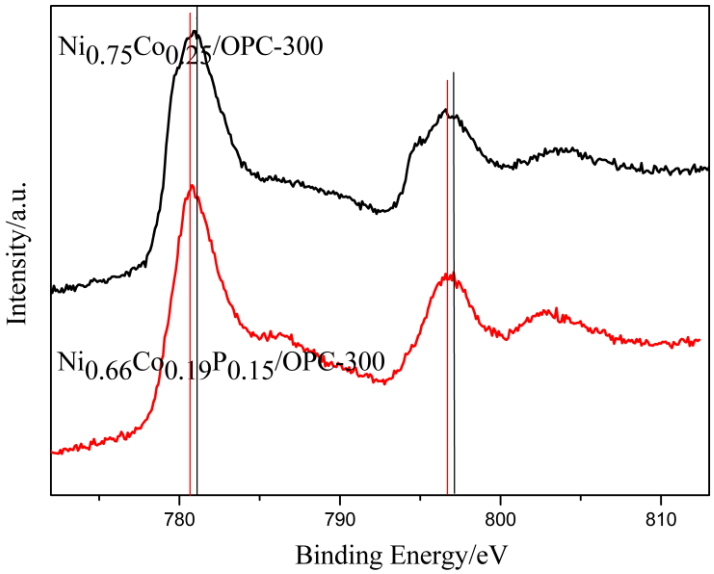

Fig.S12 Co 2p XPS spectra of $Ni_{0.66}Co_{0.19}P_{0.15}$/OPC-300 and $Ni_{0.75}Co_{0.25}$/OPC-300.

Table S3. Comparisons of recent literature results on various transition-metal-based catalysts for the hydrolysis of AB at 298K.

Catalyst	Catalyst/AB (molar ratio)	TOF ($mol_{H2}·mol_{catal}^{-1}·min^{-1}$)	Activation energy, Ea, (kJ/mol)	References
$Ni_{0.66}Co_{0.19}P_{0.15}$/OPC-300	**0.042**	**68.03[a]/95.24[b]**	**38.9**	**This work**
NiNPs@ZIF-8	0.03	35.3[a]/85.7[b]	42.7	S1
CoNPs@ZIF-8	0.03	19.4	--	S1
Ru/C	--	429.5	34.81	S2
Ru(0)@MWCNT	--	329	33	S3
Rh/graphene	0.004	325	19.7	S4
$Co_{0.32}$@$Pt_{0.68}$/C	--	248.5	41.5	S5
$Ni_{0.74}Ru_{0.26}$ alloy NPs	--	194.8	37.2	S6
Ru/graphene	0.01	100	11.7	S7
Commercial 20 wt% Pt/C	0.018	83.3	--	S8
Ag@Ni/graphene	0.05	77	49.56	S9
$Cu_{0.8}Co_{0.2}O$/GO	0.024	70	45.53	S10
$Ni_{0.9}Mo_{0.1}$/graphene	0.05	66.7	21.8	S11
40 wt % Pt/C	0.018	55.56	21-23	S12
$Cu_{0.5}Ni_{0.5}$/CMK-1	0.072	54.8	--	S13
AuNi@MIL-101	0.017	66.2	--	S14
Pd@Co@MIL-101	0.011	51(30℃)	22	S15
Co/CTF	0.03	42.3	42.7	S16
AuCo/NXC-1	0.02	42.1	31.92	S17
NiNPs@3D-G	0.009	41.7	--	S18
Ag/C/Ni	0.022	5.32	38.91	S19
RGO/Pd	0.016	6.25	51	S20
Pd/CeO_2	0.011	29	68	S21
metastable Ru NP	0.0025	21.8	27.5	S22
AuCo/CNT	0.02	36.05	38.82	S23
CoPd/C annealed	0.024	35.7	--	S24
CuPd/RGO	0.003	29.9	--	S25
Ni/γ-Al_2O_3	0.018	1.7	--	S26
Hollow-Ni NPs	0.05	4.3	--	S27
CLD-Ni/ZIF-8	0.019	8.4	--	S28
3.2 nm Ni/C	0.0425	8.8	28	S29
Nanoporous Ni spheres	0.0425	19.6	27	S30
Ni@MSC-30	0.016	30.7	--	S25
Pd/zeolite	0.02	6.25	56	S31
Co/MIL-101-1-U	0.02	51.4	31.3	S32
CuCo/MIL-101-1-U	0.02	51.7	30.5	S33
Ni0.9Mo0.1	0.05	27.3	32.1	S34

Ru/γ-Al2O3	--	23.05	67	S35
PSSA-co-MA stabilized Pd nanoclusters	--	19.9	44	S36

[a] Hydrolysis of AB in water at 298K, TOF = molH_2 released/(mol catalyst × reaction time(min)). [b] TOF is obtained in the presence of the NaOH at 298K.

As shown in Table S3, a lot of nanocatalysts have been reported for hydrogen evolution from AB, especially Ru, Rh, Pt-based noble metals and their alloys nanocatalysts have the outstanding catalytic activity among these metallic nanoparticles (MNPs) nanocatalysts[S2-S8]. Nevertheless, these noble metals and their alloys nanocatalysts could not be widely used on account of expensive costs and limited abundance. In this work, we report that the prepared noble-metal-free $Ni_{0.66}Co_{0.19}P_{0.15}$/OPC-300 nanocatalysts show the higher catalytic activity than these reported first-row late transition metal catalysts at room temperature up to now. And it is even more effective than some noble metal NPs systems such as the commercial 20 wt % Pt/C catalyst, AuNi@MIL-101and so on.

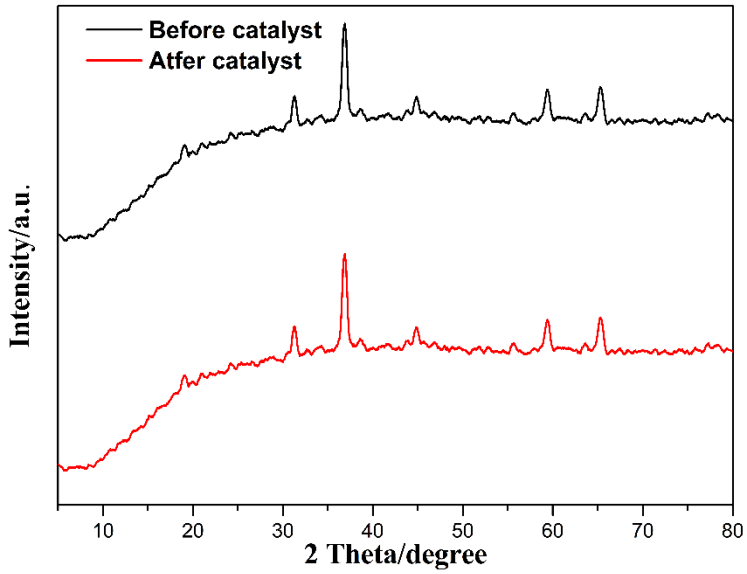

Fig.S13 PXRD patterns of the $Ni_{0.66}Co_{0.19}P_{0.15}$/OPC-300 nanocatalysts before and after 5 cycles.

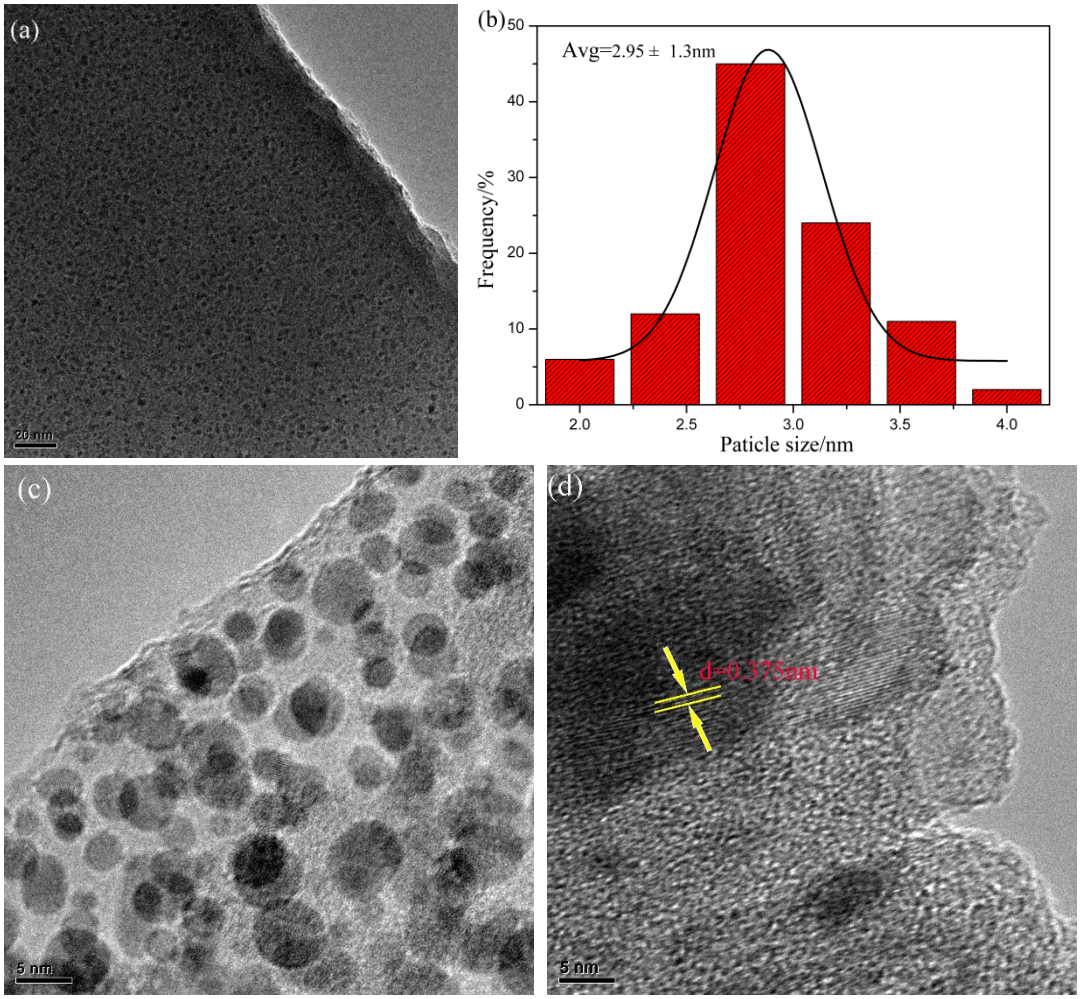

Fig.S14 TEM images of with different magnifications (a and c) of $Ni_{0.66}Co_{0.19}P_{0.15}$/OPC-300 after 5 cycles, (b) particle size distributions of the $Ni_{0.66}Co_{0.19}P_{0.15}$/OPC-300 after 5 cycles; (d) HRTEM images of the $Ni_{0.66}Co_{0.19}P_{0.15}$/OPC-300 after 5 cycles.

As shown in Fig.S14a, b, c, TEM and magnified TEM images of the $Ni_{0.66}Co_{0.19}P_{0.15}$/OPC-300 nanocatalysts after 5 cycles reveal that $Ni_{0.66}Co_{0.19}P_{0.15}$ nanoalloy particles were still well dispersed on the OPC-300 with a diameter of about 2.95±1.3 nm. By comparison, the size of $Ni_{0.66}Co_{0.19}P_{0.15}$ nanoalloy particles after 5 cycles was more than twice as large as that of $Ni_{0.66}Co_{0.19}P_{0.15}$ nanoalloy particles before the experiment. At the same time, the $Ni_{0.66}Co_{0.19}P_{0.15}$ nanocrystal after 5 cycles proves the distinct d-spacing is about 0.375nm (Fig.S14d).

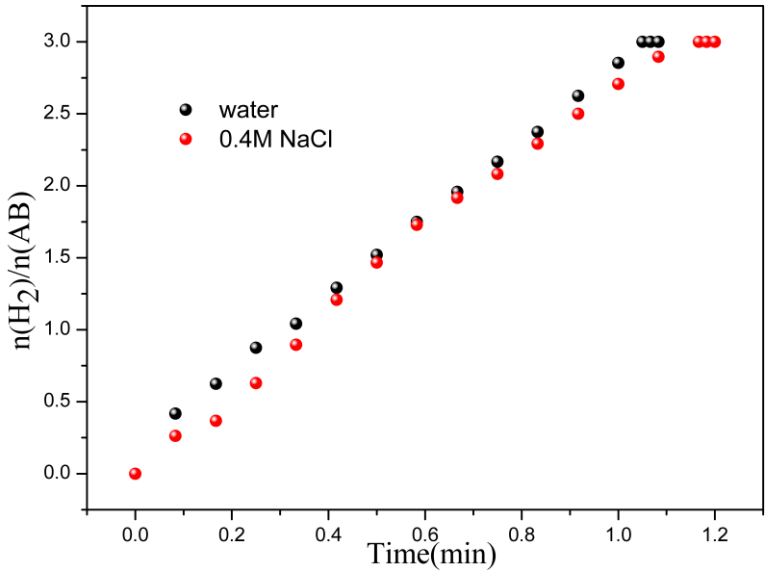

Figure.S15 Hydrogen evolution from AB by 4.2mol% $Ni_{0.66}Co_{0.19}P_{0.15}$/OPC-300 nanocatalysts in the presence of 0.4 M NaCl.

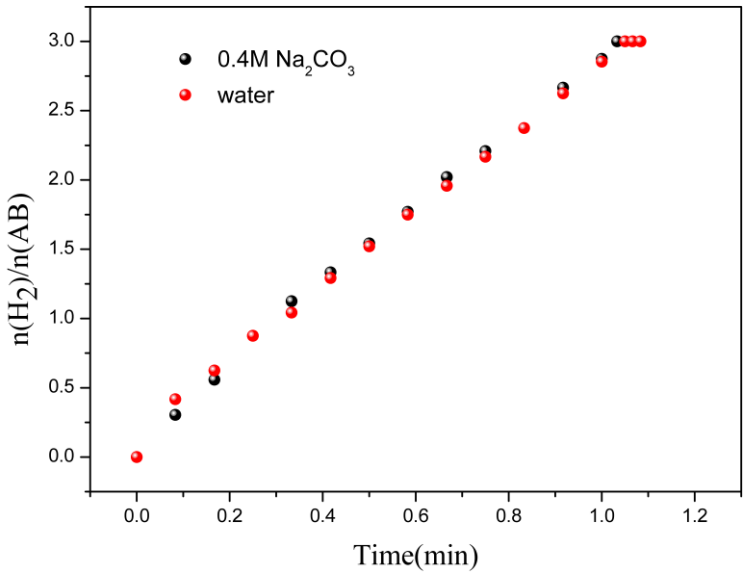

Figure.S16 Hydrogen evolution from AB by 4.2mol% $Ni_{0.66}Co_{0.19}P_{0.15}$/OPC-300 nanocatalysts in the presence of 0.4 M Na_2CO_3.

REFERENCES

S1 Changlong, W.; Jimena, T.; Zhao, W. J. Am. Chem. Soc. 2017, 139, 11610-11615.

S2 Yang ZX, Cheng FY, Tao ZL, Liang J, Chen J. Int J Hydrogen Energy 2012;37:7638-44.

S3 Wang J, Zhong HX, Qin YL, Zhang XB. Angew Chem Int Ed. 2013;52:5248-53.

S4 Shen JF, Luo W, Cheng GZ. Int J Hydrogen Energy 2015;40:1062-1070.

S5 Yang XJ, Cheng FY, Tao ZL, Chen J. J Power Sources. 2011;196:2785-9.

S6Chen GZ, Desinan S, Rosei R, Rosei F, Ma DL. Chem Eur J. 2012;18:7925-30.

S7 Cao N, Luo W, Cheng GZ. Int J Hydrogen Energy 2013;38:11964-72.

S8 M. Chandra and Q. Xu, J. Power Sources, 2006, 156, 190–194.

S9 Yang, L.; Luo, W.; Cheng, G. ACS Appl. Mater. Interfaces 2013, 5, 8231-8240.

S10 Feng, K.; Zhong, J.; Zhao, B.; Zhang, H.; Xu, L.; Sun, X.; Lee, S.-T. Angew. Chem . Int. Ed. 2016, 55, 11950-11954.

S11 Q.; Yao, Lu, Z. H.; Huang, W.; Chen, X.; Zhu, J. J. Mater. Chem. A, 2016, 4, 8579-8583.

S12 Xu, Q.; Chandra, M. J. Alloys Compd. 2007, 446, 729–732.

S13 Yen, H.; Seo, Y.; Kaliaguine, S.; Kleitz, F. ACS Catal. 2015, 5, 5505-5511.

S14 Zhu, Q.-L.; Li, J.; Xu, Q. J. Am. Chem. Soc. 2013, 135, 10210-10213.

S15 Chen, Y.-Z.; Xu, Q.; Yu, S.-H.; Jiang, H.-L. Small 2015, 11, 71-76.

S16 Li, Z.; He, T.; Liu, L.; Chen, W.; Zhang, M.; Wu, G.; Chen, P. Chem. Sci. 2017, 8, 781-788.

S17 Guo, L.; Gu, X.; Kang, K.; Wu, Y.; Cheng, J.; Liu, P.; Wang, T.; Su, H. J. Mater. Chem. A 2015, 3, 22807-22815.

S18 Mahyari, M.; Shaabani, A. J. Mater. Chem. A 2014, 2, 16652-16659.

S19 Wen, M.; Sun, B.; Zhou, B.; Wu, Q.; Peng, J. J. Mater. Chem. 2012, 22, 11988-11993.

S20 Xi, P.; Chen, F.; Xie, G.; Ma, C.; Liu, H.; Shao, C.; Wang, J.; Xu, Z.; Xu, X.; Zeng, Z. Nanoscale 2012, 4, 5597-5601.

S21 Tonbul, Y.; Akbayrak, S.; Ozkar, S. Int. J. Hydrogen Energy 2016, 41, 11154-11162.

S22 Abo-Hamed, E. K.; Pennycook, T.; Vaynzof, Y.; Toprakcioglu, C.; Koutsioubas, A.; Scherman, O. A. Small 2014, 10, 3145-3152.

S23 Kang, K.; Gu, X.; Guo, L.; Liu, P.; Sheng, X.; Wu, Y.; Cheng, J.; Su, H. Int. J. Hydrogen Energy 2015, 40, 12315-12324.

S24 Sun, D.; Mazumder, V.; Metin, O.; Sun, S. ACS Nano 2011, 5, 6458-6464.

S25 Gungormez, K.; Metin, O. Appl. Catal. A: Gen. 2015, 494, 22-28.

S26 Xu, Q.; Chandra, M. J. Power Sources 2006, 163, 364-370.

S27 Umegaki, T.; Yan, J.-M.; Zhang, X.-B.; Shioyama, H.; Kuriyama. N.; Xu, Q. J. Power Sources 2009, 191, 209-216.

S28 Li, P.-Z.; Aranishi, K.; Xu, Q. Chem.Commun. 2012, 48, 3173-3175.

S29 Metin, O.; Mazumder, V.; Ozkar, S.; Sun, S. J. Am. Chem. Soc. 2010, 132, 1468-1469.

S30 Cao, C. Y.; Chen, C. Q.; Li, W.; Song, W. G.; Cai, W. ChemSusChem. 2010, 3,1241-1244.

S31 Li, P. Z.; Aijaz, A.; Xu, Q. Angew. Chem. Int. Ed. 2012, 51, 6753-6756.

S32 Rakap, M.; Ozkar, S. Int. J. Hydrogen Energy 2010, 35, 1305–1312. S26 Liu, P.; Gu, X.;

S33 Kang, K.; Zhang, H.; Cheng, J.; Su, H. ACS Appl. Mater. Interfaces 2017, 9, 10759–10767.

S34 Yang, K.; Yao, Q.; Huang, W.; Chen, X.; Lu, Z.-H. Int. J. Hydrogen Energy 2017, 42, 6840–6850.

S35 Rachiero, G. P.; Demirci, U. B.; Miele, P. Catal. Today 2011, 170, 85−92.

S36 Metin, O.; Sahin, S.; Ozkar, S. Int. J. Hydrogen Energy 2009, 34, 6304−6313.